12

Resistive plate chambers

12.1 Spark counters

In wire-based detectors, an intrinsic limitation to the achievable time resolution is set by the statistical distribution of the primary ionization clusters, combined with the dispersions due to diffusion in the time needed to drift and amplify the ionization charge at the anode. As discussed in Chapter 6, in a parallel plate counter (PPC), where multiplication occurs immediately after the release of primary electrons in the gas, the charge signals are detected on electrodes without a delay and can therefore provide a much better time resolution. However, this requires detecting the induced signals at the very beginning of the avalanche development; good results can only be obtained with large multiplication factors, obtainable at very high fields. In a standard PPC with conductive electrodes this is a critical operation, seriously hindered by discharges and their propagation throughout the whole counter.

A structure capable of achieving the required high gains while limiting the discharge propagation, named the spark counter, employs one or two high-resistivity electrodes; the large current surge generated by an avalanche then results in a localized field drop, thus dumping the discharge (Pestov, 1982). Operation near to or in the discharge mode is then possible, and provides fast and large signals. Localization can be conveniently performed with external readout strips or pads in contact with the outer face of the resistive electrodes.

Use of a gas mixture designed to absorb photons in a wide energy range avoids propagation and ensures the locality of the discharge; Figure 12.1 is an example of the combined photon absorption coefficients for the mixture with the components and proportions indicated in the inset (Pestov *et al*., 2000).

A narrow gap (100 to 300 μm), which requires high fields for multiplication, reduces the statistical fluctuations in the avalanche development, and provides the best time resolution; it imposes, however, constraints to the quality and uniformity

https://doi.org/10.1017/9781009291200.014 Published online by Cambridge University Press

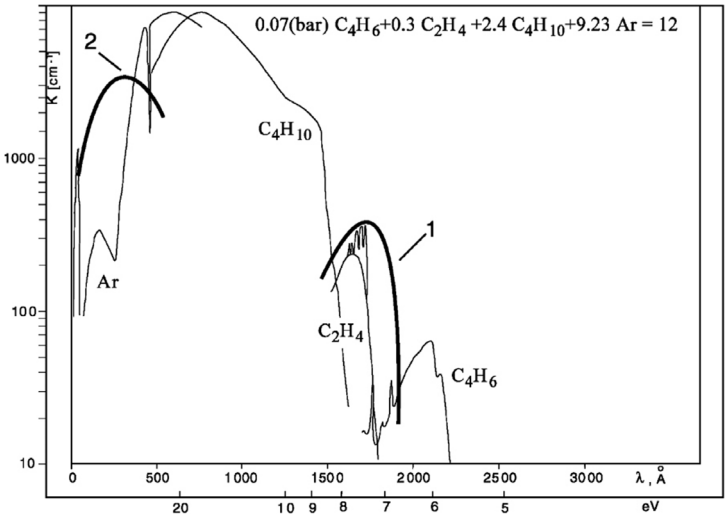

Figure 12.1 Combined photon absorption coefficient/cm of the gas mixture shown in the inset as a function of photon energy and wavelength (Pestov *et al.*, 2000). By kind permission of Elsevier.

of the electrodes. For detection of minimum ionizing particles, to compensate for the reduced efficiency due to the energy loss statistics in a narrow gap, the counter can be operated at high pressures.

By using as cathode a custom-made electron conducting glass with resistivity in the range 10^9 to $10^{10}\Omega$ cm (see Section 13.1), a 100 μm gap and a complex mixture of hydrocarbons at 12 bars, time resolutions down to 30 ps have been demonstrated in the early 1980s (Pestov, 1982); Figure 12.2 is the outcome of systematic time resolution measurements achieved with different gas mixtures; the horizontal scale is the ratio of the operating to the multiplication threshold voltages.

Electrostatic properties of spark counters as well as the signal propagation in transmission lines on resistive supports have been studied in detail, aiming at the construction of large size detectors (Steinhaeuser *et al.*, 1997). Reviews of the technology and its applications are given in Schmidt (1999) and Pestov (2002); the second reference includes a critical comparison of performances of resistive plate detectors built with a range of electrode materials and in different modes of operation, from avalanche to spark.

The difficult procurement of the electron-conducting glass and the high pressures of operation, requiring heavy gas containment vessels, have, however, discouraged the use of the technology; nevertheless the main findings of the development constituted the basis for further developments of parallel plate counters. The electron-conducting glass (also named Pestov glass) has been also used successfully in the development of high-rate microstrip chambers, described in Section 13.1.

https://doi.org/10.1017/9781009291200.014 Published online by Cambridge University Press

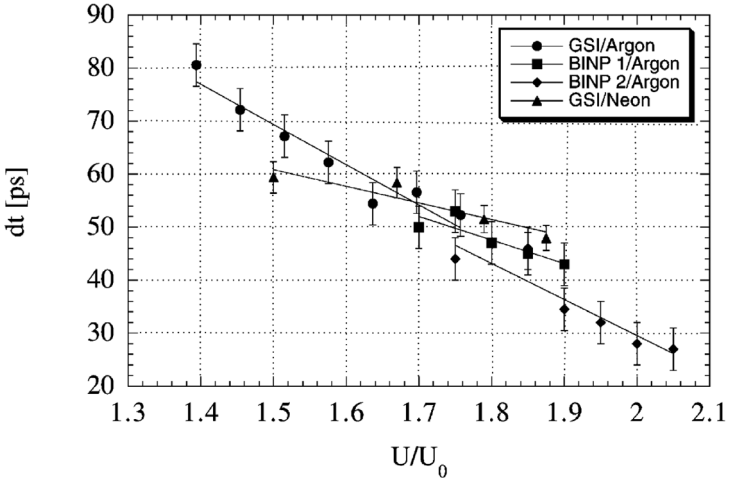

Figure 12.2 Time resolution of a spark counter measured for fast particles in several beam runs and gas mixtures, as a function of relative over-voltage (Pestov *et al*., 2000). By kind permission of Elsevier.

12.2 Resistive plate counters (RPCs)

Aiming at the realization of very large detection areas, the resistive plate counters (RPC) employ high-resistivity electrodes made of phenolic polymer laminates, which are cheap and easily available, and have a volume resistivity between 10^9 and $10^{10}\Omega$ cm.[1] With sensitive gas gaps a few mm thick, RPCs achieve full detection efficiency and nanosecond time resolutions for fast particles (Santonico and Cardarelli, 1981; Cardarelli *et al*., 1988). Further developments have permitted one to consolidate the technology and build the very large systems, hundred of square meters in area, needed for muon detection in high-energy physics experiments.

Figure 12.3 is a schematic cross section of a standard single-gap RPC. The high resistivity electrode plates are assembled with insulating support frames, providing tightness and gas distribution; for large detector sizes, regularly spaced insulating pillars between the electrodes ensure the uniformity of the gap. To provide the operating voltage over large detection areas and avoid the potential drops caused by the signal currents, the plates are coated on the outer side with a thin graphite layer having a moderate surface resistivity, around 200–300 kΩ/square[2] that

[1] Common trade names: Bakelite, Melamine; the value of the resistivity can be controlled with additives.

[2] The resistance of a uniformly conductive slab of thickness L between two faces of surface A is given by the expression $R = \rho L/A$, where ρ is the bulk resistivity (in Ω cm). For thin conductive sheets of thickness s, the sheet resistance is defined as $R_s = \rho/s$, usually expressed in Ω/square since its value is independent of the size of the square.

https://doi.org/10.1017/9781009291200.014 Published online by Cambridge University Press

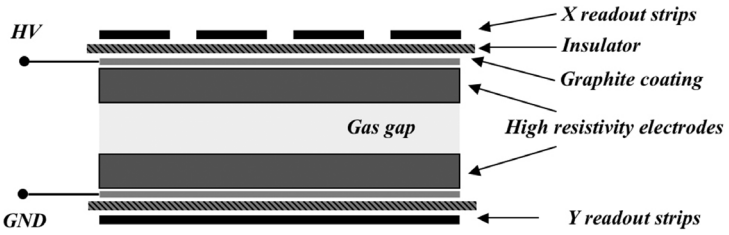

Figure 12.3 Schematics of a resistive plate chamber.

distributes the potentials while permitting detection of the signals induced by the avalanche multiplication on sets of external strips, insulated from the electrodes (see also the discussion on electrode transparency in Section 11.1).

On application of a voltage to the coatings, a migration of charges in the bulk of each electrode cancels the external field, making them equi-potential, so that the full field gradient is applied across the gas layer. As discussed in detail in Chapter 5, following the passage of an ionizing particle and under the effect of the electric field, starting from each primary ionization cluster charge-amplifying avalanches develop in the gas, and add up to build the entire signal; for a few mm thick gap, the process takes 10 ns or less. Due to the exponential avalanche growth, the largest fraction of the detected charge originates from the ionization electrons closer to the cathode; for a discussion of the signal formation process in parallel plate counters, see Section 6.4.

When the avalanche size exceeds 10^6–10^7 electrons, the exponential growth is damped due to the field reduction induced by the growing space charge; this leads to a saturated avalanche regime. On increasing the voltage further, a transition to a streamer may occur; this operating mode was exploited in the early developments, owing to the conveniently large signals obtained, but implies a reduction in the rate capability of the detector caused by the large local voltage drop, only slowly recovering through the high resistivity of the electrodes. A comparison of detection efficiency in the avalanche and streamer modes as a function of particle flux is shown in Figure 12.4 (Arnaldi *et al.*, 1999); in the streamer mode the maximum flux for efficient detection is reduced by several orders of magnitude.

The rate dependence of detection efficiency can be described by a simple model that takes into account only the local drop of effective potential due to the avalanche currents; Figure 12.5 compares the results of the simulation with experimental measurements realized on a standard bakelite RPC with 2 mm gap and bulk resistivity $8 \times 10^{10}\Omega$ cm (Abbrescia, 2004).

To achieve high and stable gains, RPCs are operated with heavily quenched, photon-absorbing gases, as freon (CF_3Br) or mixtures of tetrafluoroethane ($C_2H_2F_4$) and isobutane (i-C_4H_{10}) (Cardarelli *et al.*, 1993; Cardarelli *et al.*, 1996); heavily

https://doi.org/10.1017/9781009291200.014 Published online by Cambridge University Press

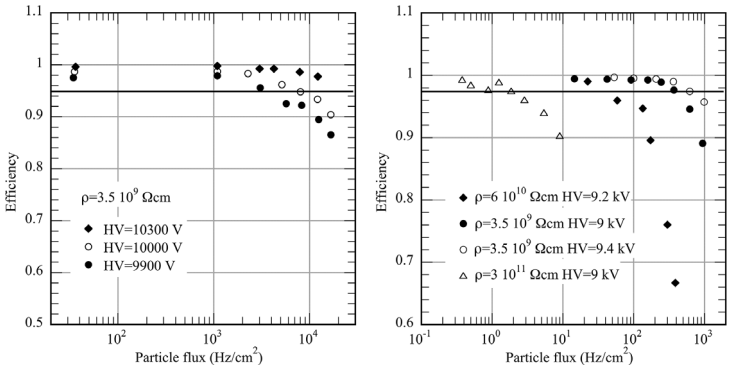

Figure 12.4 RPC efficiency as a function of particle flux and voltage in the avalanche (left) and streamer modes (right) for several values of bulk resistivity (Arnaldi *et al.*, 1999). By kind permission of Elsevier.

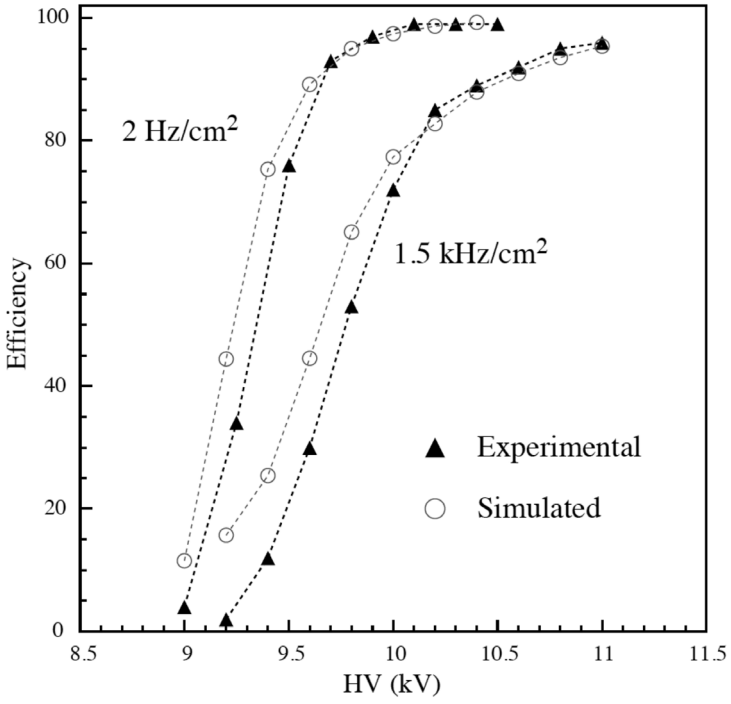

Figure 12.5 Simulated and measured efficiency for minimum ionizing particles at two values of flux (Abbrescia, 2004). By kind permission of Elsevier.

quenched argon-based mixtures are used to reduce the voltage needed for operation (Wang, 2003; Bergnoli *et al.*, 2009; Zhang *et al.*, 2010).

While the streamer mode offers a substantial advantage in terms of signal charge, for many applications an operation in the saturated avalanche mode is

https://doi.org/10.1017/9781009291200.014 Published online by Cambridge University Press

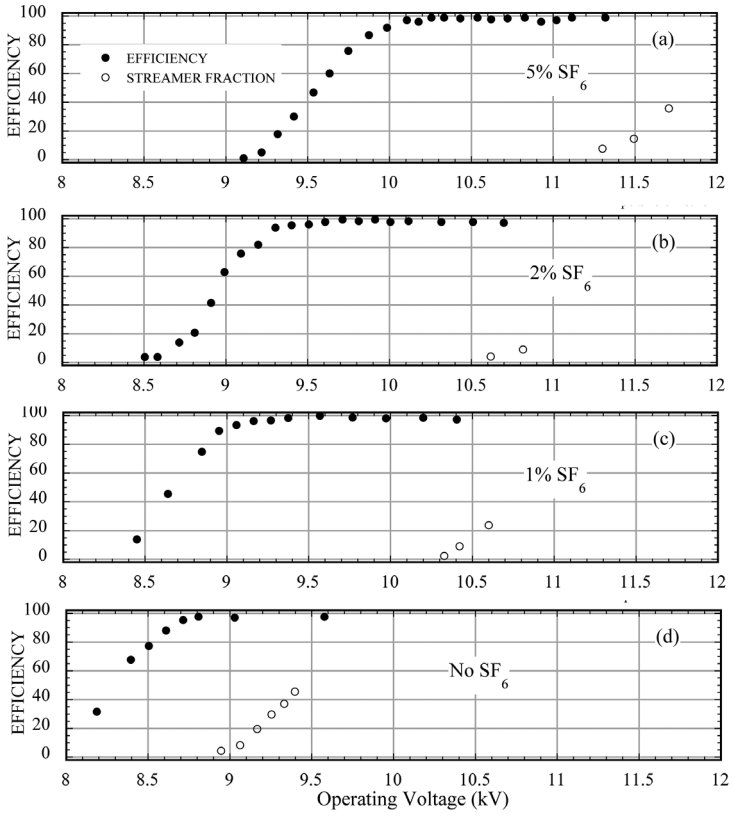

Figure 12.6 Efficiency plateau and streamer onset probability as a function of voltage for several percentages of SF_6 addition to the gas (Camarri *et al.*, 1998). By kind permission of Elsevier.

preferred to avoid efficiency losses in the high flux areas of the detector. In this case, owing to the inevitable differences in local gain due to mechanical tolerances, it is mandatory to ensure that the onset of the streamer mode appears at a voltage sufficiently above the one required for normal operation.

The influence of the gas filling on the length of the plateau in the avalanche mode before the streamer has been studied extensively. Addition of small percentage of an electro-negative gas to the mixture considerably increases the gap between the avalanche and streamer modes, as shown in Figure 12.6 for several percentages of sulphur esafluoride (SF_6) added to a $C_2H_2F_4$-C_4H_{10} mixture (Camarri *et al.*, 1998).

The streamer suppression effect of the addition of small percentages of SF_6 has been confirmed by many systematic studies, motivated by the development of reliable RPCs for massive use as muon detectors in large experiments. Figure 12.7

https://doi.org/10.1017/9781009291200.014 Published online by Cambridge University Press

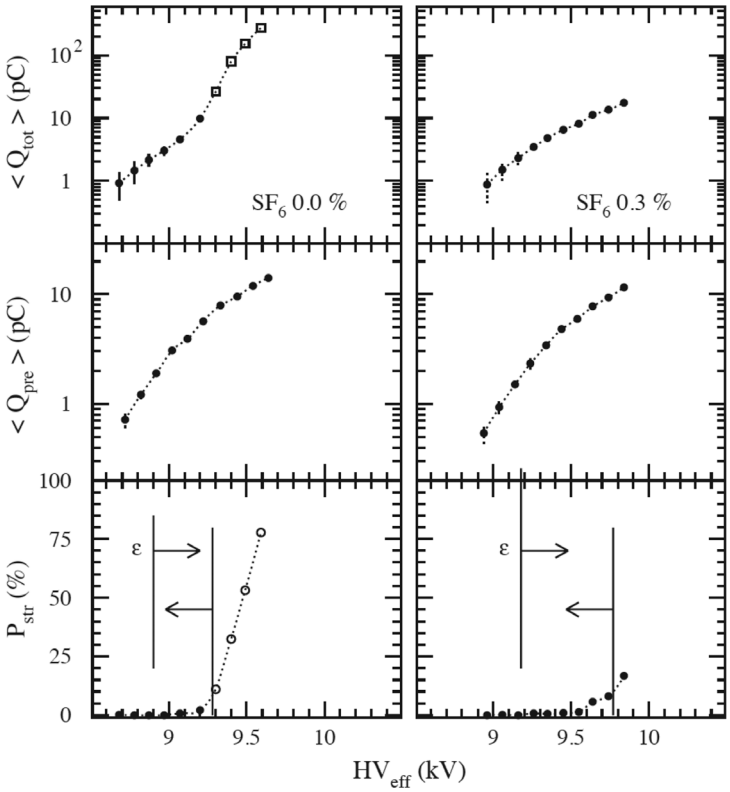

Figure 12.7 Average (top) and streamer precursors total charge (middle) as a function of voltage without and with SF_6 in the gas mixture. The bottom plots show the streamer onset probability (Ahn *et al.*, 2004). By kind permission of Elsevier.

is a representative example (Ahn *et al.*, 2004); this study includes a comparison of the experimental results with a simple avalanche multiplication model. As already mentioned, addition of the quenchers to argon in various proportions permits one to lower the operating voltage, with obvious practical advantages.

The use of cheap phenolic resin electrodes, while permitting the realization of very large detectors, is hindered by the modest surface quality of the material, thus inducing local spontaneous discharges and leading to high background noise. While several methods of surface treatment have been investigated, a simple solution to the problem was found at the early stage of development by wetting the electrodes with linseed oil dissolved in alcohol, having the property to form a thin, high resistivity polymer coating when drying, covering the surface imperfections (Santonico and Cardarelli, 1981). The considerable reduction in noise rate that can be obtained with the linseed oil conditioning is shown by the comparison

https://doi.org/10.1017/9781009291200.014 Published online by Cambridge University Press

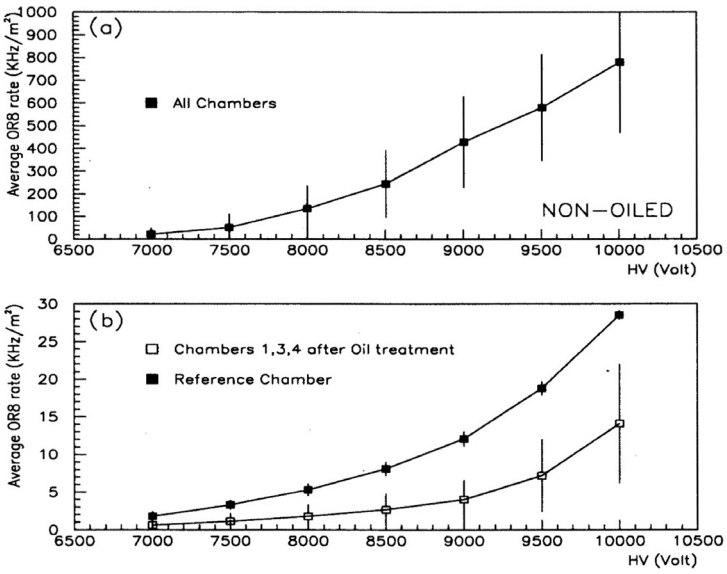

Figure 12.8 Noise rate comparison between non-oiled (a) and two linseed oil treated RPCs (Abbrescia *et al.*, 1997). By kind permission of Elsevier.

in Figure 12.8 (Abbrescia *et al.*, 1997). Despite serious problems encountered in BaBar at SLAC, one of the first experiments making large use of linseed-coated bakelite RPCs, and related to incomplete polymerization, formation of droplets on the surface and on the internal pillars used as gap-restoring spacers (Anulli *et al.*, 2002), with various improvements the technology has been successfully adopted in a majority of RPC-based experimental setups. A long-term decrease in rate capability during operation, imputed to a gradual increase of the electrodes' resistivity with exposure to radiation and/or moisture has also been observed. More detailed studies of long-term degradation (ageing) of RPCs are discussed in Chapter 16.

For a comparison of performances between detectors manufactured with several types of bakelite laminates, with and without the linseed oil conditioning, see for example Biswas *et al.* (2009). Essential to guarantee stable long-term operation of the detectors, the temperature and humidity dependences of the materials' bulk resistivity have been studied systematically by many authors (Ahn *et al.*, 2000; Aielli *et al.*, 2004; Aielli *et al.*, 2006; Doroud *et al.*, 2009b; Moshaii and Doroud, 2009).

RPCs have been produced industrially in massive quantities for use as muon detectors in many large particle physics experiments and are amply described in the literature: BaBar at SLAC (Ferroni, 2009), OPERA (Bertolin *et al.*, 2009), CMS (Colaleo *et al.*, 2009), ATLAS and ALICE at CERN (Bindi, 2012; Arnaldi *et al.*, 2009), BESIII at the Beijing Electron-Positron Collider (Zhang *et al.*, 2010)

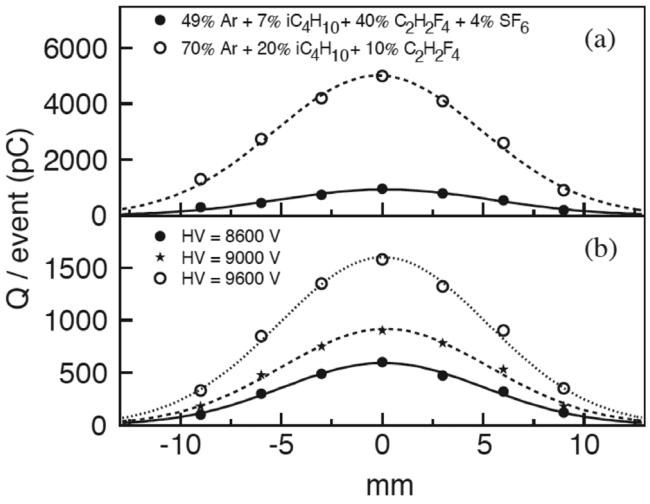

Figure 12.9 Charge profiles recorded in various conditions on a low-resistivity bakelite RPC operated in the streamer mode (Arnaldi *et al.*, 2002). By kind permission of Elsevier.

and many others. The ARGO-YBJ RPC array in Tibet, aimed at the detection of extended cosmic air showers, deploys about 2000 RPC modules covering a sensitive area of 6700 m^2 (Camarri, 2009). Performances and long-term operating stability are described in a vast number of works; good sources of information are the proceedings of regular International Resistive Plate Chambers International Workshops (RPC2005, 2006; RPC2007, 2009) and numerous reviews (Santonico, 2009; Sharma, 2009; Santonico, 2012; Sharma, 2012).

The space distribution of the signals induced on the external electrodes depends on the detector geometry, thickness of the electrodes and operating conditions. Since the induction process is very fast compared to the local RC of the detectors, the resistivity of the electrode has only a small effect on the width, as it can be inferred by simple electrostatics consideration and confirmed by measurements (Arnaldi *et al.*, 2000). Figure 12.9 is an example of charge profiles measured with a low resistivity (~$10^9\Omega$ cm) bakelite RPC for various gas mixtures and voltages; a Gaussian fit to the distributions gives a standard deviation of about 5 mm, close to the distance between the avalanche maximum in the detector and the pickup strips (Arnaldi *et al.*, 2002). This result is reminiscent of similar observations with MWPCs (see the discussion on the pad response function in Section 10.4).

Recording the charge induced through the electrodes on readout strips or pads provides the time of the event and the space coordinates of tracks crossing the detector; in large area devices, the strip width is typically a few cm, to reduce the number of readout channels and the sharing of charge between adjacent strips.

https://doi.org/10.1017/9781009291200.014 Published online by Cambridge University Press

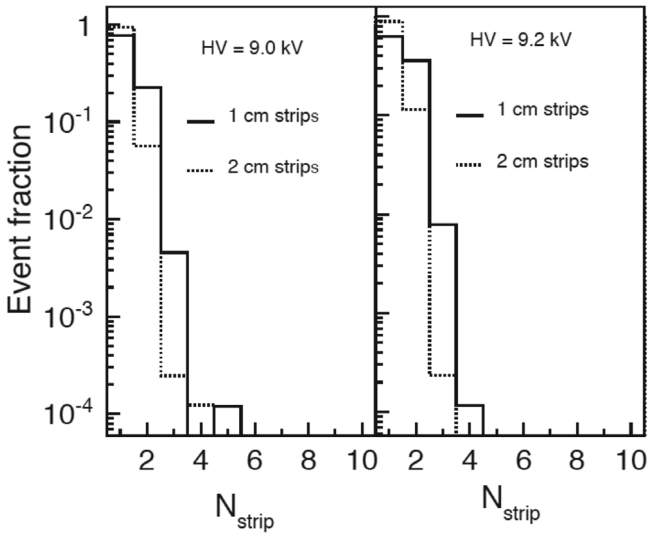

Figure 12.10 Distribution of the number of fired strips for 1 and 2 cm width (Arnaldi *et al*., 2002). By kind permission of Elsevier.

Figure 12.10, from the previous reference, shows the measured distributions of the number of strips above threshold (or cluster size) for two strip widths and two values of operating voltage; for 1 cm wide strips, the probability of double hit events is about 20%, slightly increasing with voltage.

For a digital readout, the localization accuracy for single strip hit is simply given by $w/\sqrt{12}$, where w is the strip pitch; in the case of charge sharing between adjacent strips, or for the wider clusters induced by inclined tracks, the localization accuracy is improved by making suitable averages (Carrillo, 2012).

The time resolutions achievable with RPCs depend, amongst other factors, on their operating voltage and gap thickness; measured with a low resistivity detector ($\sim 5\ 10^9\ \Omega$cm) in the avalanche mode, Figure 12.11 is a representative example, with better than 1 ns standard deviation (Arnaldi *et al*., 1999). For the large RPC-based systems built for experiments at CERN's LHC, a few ns resolution is sufficient to resolve two beam crossings at 25 ns. Better time resolutions, well below 100 ps and suitable for particle identification, are obtained with the narrow gap RPCs discussed in the next section.

12.3 Glass RPCs

Alternatively to the use of phenolic laminates as resistive electrodes, and close to the original development of spark counters described in Section 12.1, a concurrent approach uses plates of float glass as electrodes, available in a wide range of sizes

https://doi.org/10.1017/9781009291200.014 Published online by Cambridge University Press

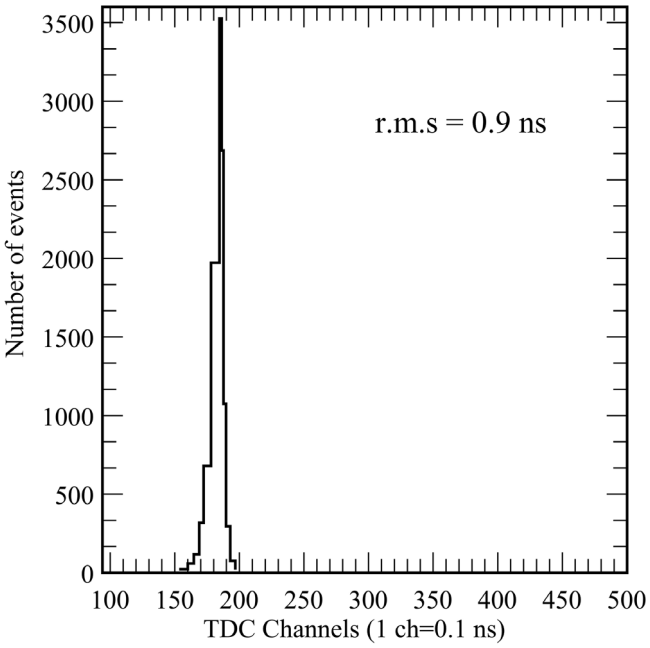

Figure 12.11 Time resolution measured for fast particles of a low resistivity, 2 mm gap RPC (Arnaldi *et al.*, 1999). By kind permission of Elsevier.

and thickness with a resistivity of 10^{11}–10^{12} Ω cm; the operating voltage is also provided by a lower resistivity layer, typically of about 1 MΩ/square deposited on the outer surface of the glass (Anelli *et al.*, 1991; Gustavino *et al.*, 2001; Trinchero *et al.*, 2003). As for the higher conductivity materials, at the application of the external electric field, free charges within the glass (presumably ions) migrate and rearrange, thus creating an internal field opposing the applied field and making the plates equi-potential.

A clear advantage of glass, compared to Bakelite, is its very good surface smoothness, therefore not requiring special conditioning; the drawback, due to the high resistivity, is a limited rate capability. This is, however, compensated by a more stable operation with time (Calcaterra *et al.*, 2004; Candela *et al.*, 2004). High resistivity glass is also used for the electrodes of multi-gap RPCs, discussed in the following section.

In the large glass RPC system built for the BELLE experiment at KEK, commercially available, 2.4 mm thick float glass plates were used, with bulk resistivity in the range 10^{12}–10^{13} Ω cm, coated with a custom-made India ink layer having a surface resistivity of 10^{6}–10^{7} Ω/square to distribute the high voltage (Wang, 2003). Similar detectors have been built for DAΦNE at the Frascati INFN

https://doi.org/10.1017/9781009291200.014 Published online by Cambridge University Press

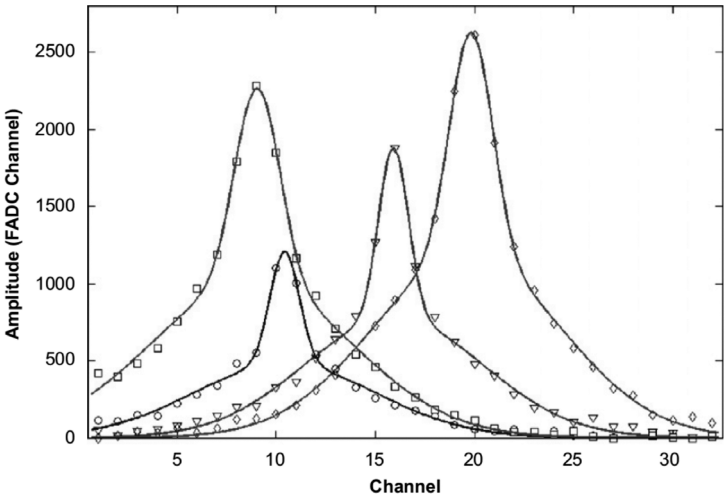

Figure 12.12 Charge profiles for several events recorded on 1 mm wide strips (Ye *et al.*, 2008). By kind permission of Elsevier.

laboratory (Calcaterra *et al.*, 2004), for a digital calorimeter of the International Linear Collider (Bedjidian *et al.*, 2010).

Sub-mm localization accuracies can be achieved with the use of thin electrodes and small pitch readout strips; Figure 12.12 is an example of charge profiles recorded on a 1 mm wide adjacent strips on a detector made with 700 μm thick glass and 2 mm gas gap. The characteristic double Gaussian shape of the distributions is attributed to a narrow signal induced by the avalanches, adding to a wider dispersion due to the low-resistivity external carbon layer used to distribute the voltage; a fit to the narrower distribution provides a position accuracy around 500 μm (Ye *et al.*, 2008).

The use of a custom-made lower resistivity glass (~10^{10} Ω cm) permits one to preserve detection efficiency at the higher rates foreseen for the LHC upgrade; Figure 12.13 is a comparison of measured detection efficiency as a function of particle flux for standard and low resistivity glass detectors (Haddad *et al.*, 2013).

Surface damage to the electrodes due to a reaction of water with fluorinated compounds released in the avalanche processes have been experienced in the BELLE experiment at KEK (T. Kubo *et al.*, 2003); more recent observations of the damaging effect of carbon tetrafluoride on glass are discussed in Chapter 16.

12.4 Multi-gap RPCs

In RPCs operated at atmospheric pressure, a few mm thick gas gaps are needed to ensure full detection efficiency for minimum ionizing particles. With an average

https://doi.org/10.1017/9781009291200.014 Published online by Cambridge University Press

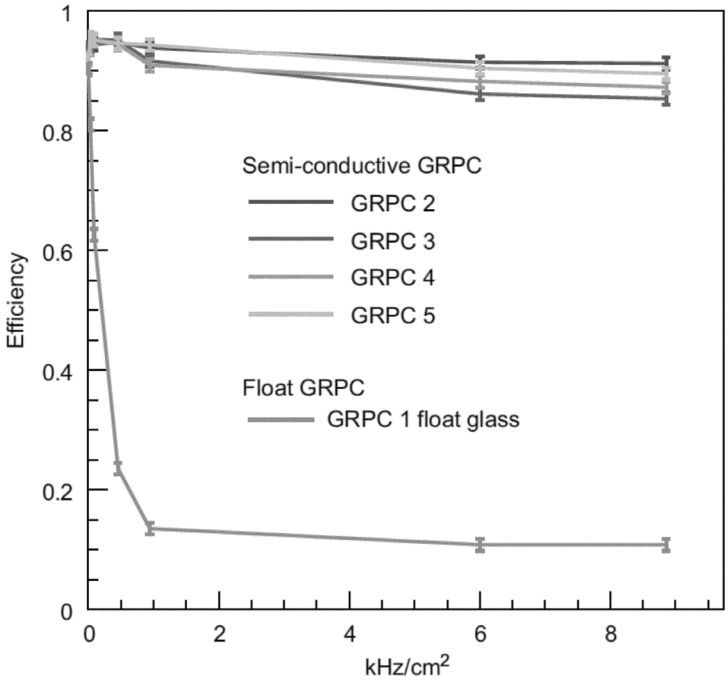

Figure 12.13 Comparative efficiency measured as a function of flux for standard float glass and several lower resistivity devices (Haddad *et al.*, 2013). By kind permission of Elsevier.

distance between primary ionizing collisions of around 300 μm, and since the avalanche size depends on the distance of the ionization clusters from the anode, the ensuing fluctuations limit the intrinsic time resolution of the detectors to a few ns. A substantial improvement in time resolution is achieved by reducing the gap thickness; however, this goes at the expense of the detection efficiency (Zeballos *et al.*, 1996).

The multi-gap RPCs (MRPCs), combining in a single device a stack of interconnected and narrow gap modules, permits one to achieve at the same time good efficiency and time resolution (Cerron-Zeballos *et al.*, 1996; Fonte *et al.*, 2000). Initially manufactured with individually powered resistive plates, the concept evolved with the discovery that, on application of the high voltage only to the external plates in a multi-gap stack, the intermediate floating electrodes reach the appropriate equilibrium potential dynamically and do not need to be connected, as shown schematically in Figure 12.14; this greatly simplifies the detector construction (Akindinov *et al.*, 2000). For large sizes, thin fishing lines stretched across the gaps ensure gain uniformity and prevent the deformations due to electrostatic forces.

Each gap then operates independently; avalanches develop following the release of ionization, and equal and opposite polarity signals are induced through the stack

https://doi.org/10.1017/9781009291200.014 Published online by Cambridge University Press

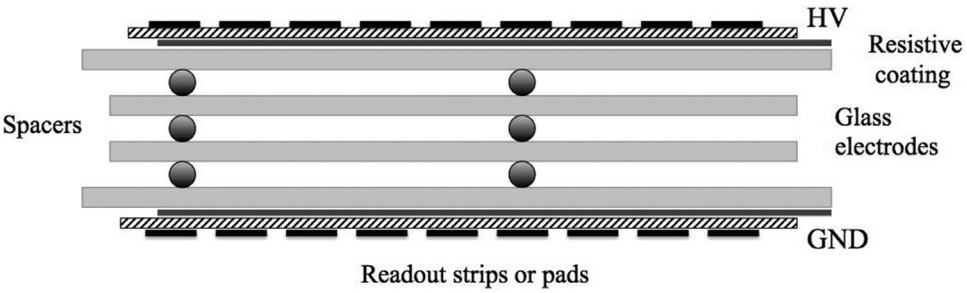

Figure 12.14 Schematics of a five-gap MRPC. The operating voltage is applied to resistive layers applied on the outer plates; signals are detected on external insulated circuits.

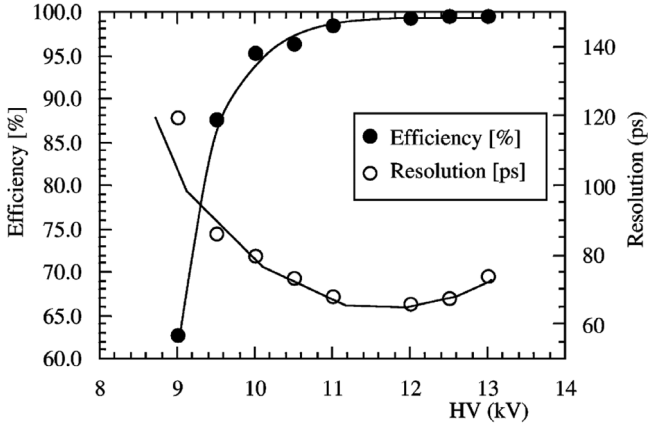

Figure 12.15 Efficiency and time resolution as a function of voltage for a five-gap MRPC (Akindinov *et al.*, 2000). By kind permission of Elsevier.

on the external electrodes; the larger and faster signals determine the time resolution of the structure. Figure 12.15 shows the efficiency and time resolution measured for fast particles as a function of voltage with a five 220 μm thick gaps MRPC built on thin high-resistivity glass plates; the gas filling is a mixture of 90% $C_2F_4H_2$, 5% i-C_4H_{10} and 5% CF_4 (Akindinov *et al.*, 2000).[3]

While limited in rate due to the very high resistivity of the glass electrodes, the structure reacts to the creation of regions of high space charge with a local reduction of gain, making the operation stable.

Thanks to the excellent time resolution achieved, glass MRPCs are used to perform particle identification through a measurement of time-of-flight by the

[3] Later studies with the same structures have demonstrated that similar performances can be obtained using only $C_2F_4H_2$ as gas filling.

https://doi.org/10.1017/9781009291200.014 Published online by Cambridge University Press

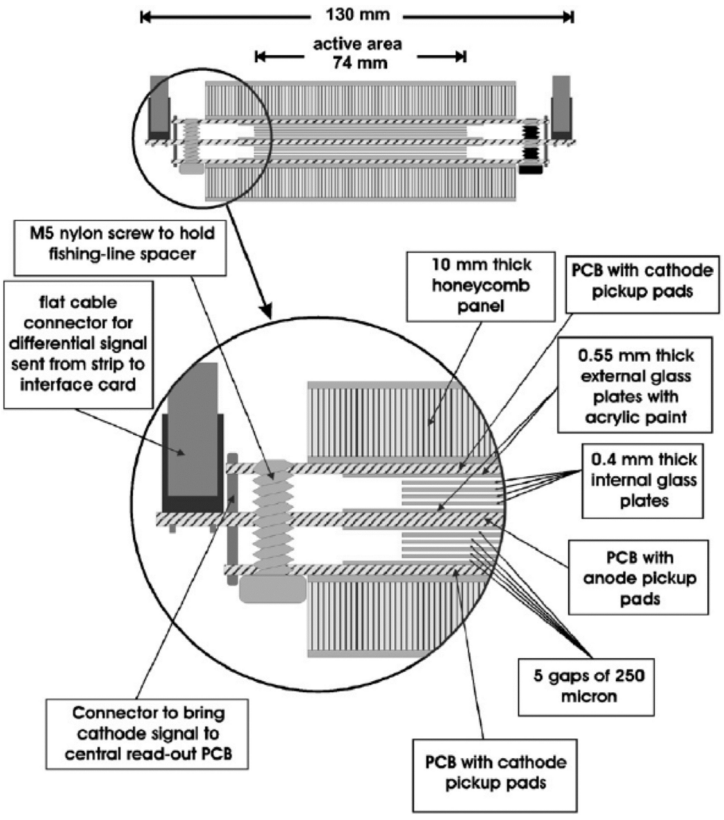

Figure 12.16 Schematics of the ALICE MRPC TOF module (Akindinov *et al.*, 2004). By kind permission of Elsevier.

ALICE experiment at LHC. The resistive plates are made with soda-lime glass plates, 400 μm thick; spacers made with nylon fishing lines 250 μm in diameter ensure the gap uniformity. Figure 12.16 shows a general and detailed schematic of a dual ALICE TOF module (Akindinov *et al.*, 2004); assembled in modules 120×7.4 cm^2 with two stacks of five gaps each, the detectors are read out by arrays of rectangular pads placed on the central and outer surface of the stack.

Measured for fast particles with a set of fast scintillators as time reference, Figure 12.17 shows the efficiency and the standard deviation of the time resolution of the module as a function of voltage.

Crucial to achieve sub-ns time resolutions is the use of very fast amplifiers-discriminators; due to the wide charge spectrum of signals generated in parallel plate detectors, a time walk correction of the recorded time, taking into account the signal amplitude, is needed for best results. To achieve this goal, a dedicated ASIC chip developed for the needs of the ALICE TOF project, named NINO, has eight channels of low-noise, fast amplifiers-discriminators with adjustable threshold

https://doi.org/10.1017/9781009291200.014 Published online by Cambridge University Press

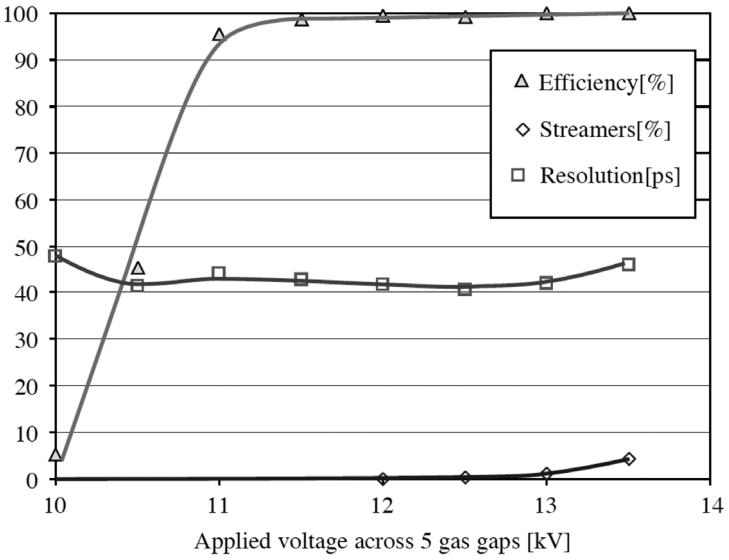

Figure 12.17 Efficiency and time resolution of the ALICE MRPC dual five-gap module (Akindinov *et al.*, 2004). By kind permission of Elsevier.

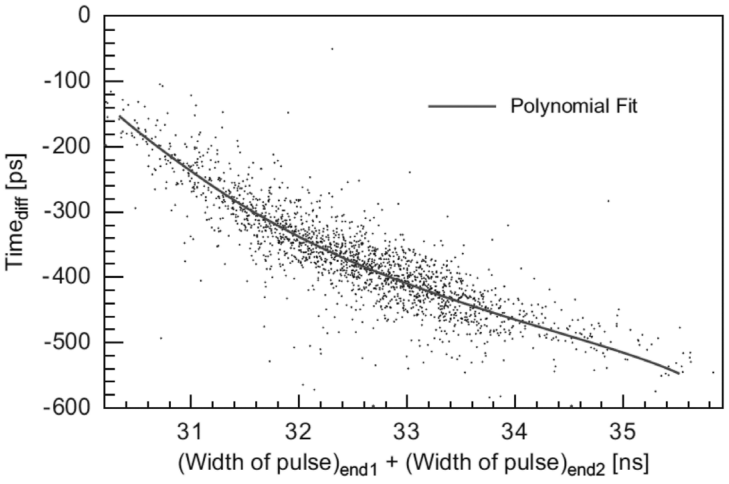

Figure 12.18 Correlation between recorded time and discriminator pulse width, used for time slewing corrections (An *et al.*, 2008). By kind permission of Elsevier.

(Anghinolfi *et al.*, 2004). To improve the signal over noise ratio, the circuit has a differential input, connected to two sets of parallel readout strips on each side of the detector. The recorded width of the discriminated output, proportional to the signal charge, is used for slewing correction. Measured with a 24-gap MRPC, Figure 12.18 is a scatter plot of the measured dependence of the relative time

https://doi.org/10.1017/9781009291200.014 Published online by Cambridge University Press

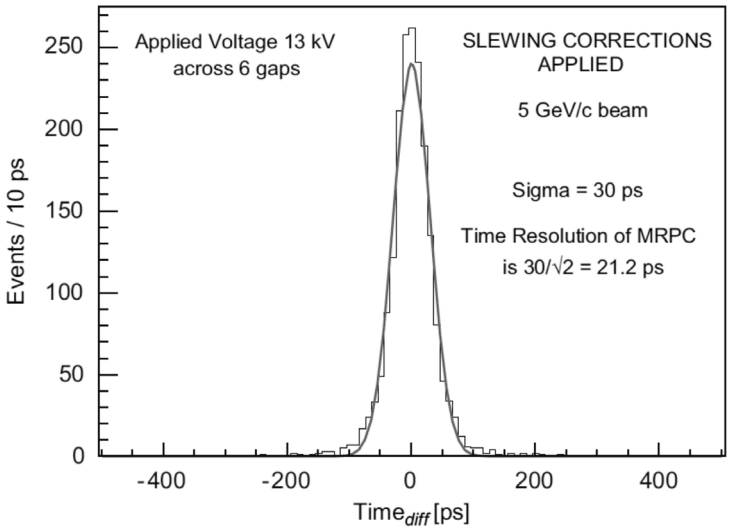

Figure 12.19 Time difference for fast particles between two MRPCs after slewing correction (An *et al*., 2008). By kind permission of Elsevier.

measurement from the discriminator pulse width. The correction spans over about several hundred ps, to be compared with the best achieved TOF resolution of around 30 ps, see Figure 12.19 (An *et al*., 2008).

Based on the glass MRPC described, the ALICE TOF detector is a modular structure with 18 sectors covering the full azimuthal angle and five segments in the longitudinal coordinate along the beam axis; the MRPCs are housed in gas tight modules and assembled in groups of five constituting a 'supermodule'. The picture in Figure 12.20 shows one of the supermodules prior to installation (Akindinov *et al*., 2009); Figure 12.21 illustrates the particle identification power of the detector, combining TOF with the particle momentum measured by magnetic deflection (Akindinov *et al*., 2012).

12.5 Simulations of RPC operation

Aimed at improving the time and localization properties of the detectors, detailed studies of signal formation and induction process on external electrodes, reproducing the observed signal spectra, have been described. Many authors have investigated the physics of the avalanche development mechanisms in detectors with resistive electrodes, with both analytic calculations and simulation models, analysing the effects of ionization statistics, gap thickness and field modifications due to space charge and negative ion formation due to attachment to electro-negative gas molecules.

https://doi.org/10.1017/9781009291200.014 Published online by Cambridge University Press

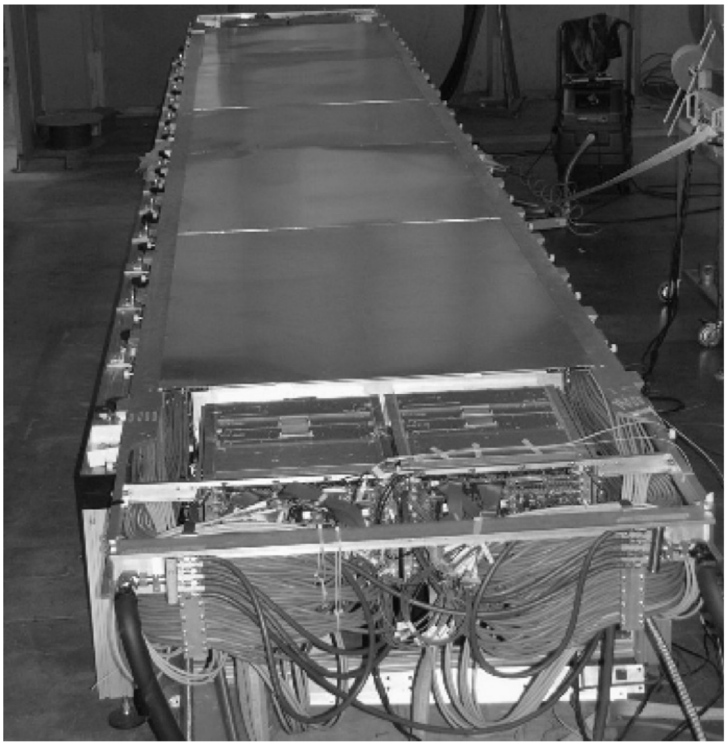

Figure 12.20 One of the MRPC supermodules of the ALICE TOF system (Akindinov *et al*., 2009). By kind permission of Elsevier.

The calculation of the avalanche development and propagation can be done analytically (Ammosov *et al*., 1997; Mangiarotti *et al*., 2004) or with Monte Carlo simulation programs, taking into account the strong effect of the space charge at the very high values of fields, typically above 100 kV/cm, met in RPC (Abbrescia *et al*., 1999a; Abbrescia *et al*., 1999b; Nappi and Seguinot, 2005; Lippmann and Riegler, 2004; Riegler, and Lippmann, 2004; Khorashad *et al*., 2011). As an example, Figure 12.22 shows the good agreement between the measured charge spectra with the results of a numerical calculation (Lippmann and Riegler, 2004).

The avalanche growth as a function of time in the MRPC has been simulated using the program MAGBOLTZ (Biagi and Veenhof, 1995b) and with the algorithms developed by Lippmann and Riegler (2004), taking into account the creation of negative ions in the gas containing electro-negative molecules. An example of the results is shown in Figure 12.23, the evolution of the charge density and of the electric field in the gap at successive time intervals following the ionization process (Doroud *et al*., 2009a). The high density of negative ions and consequent recombination with the positive ions generated in the avalanches

https://doi.org/10.1017/9781009291200.014 Published online by Cambridge University Press

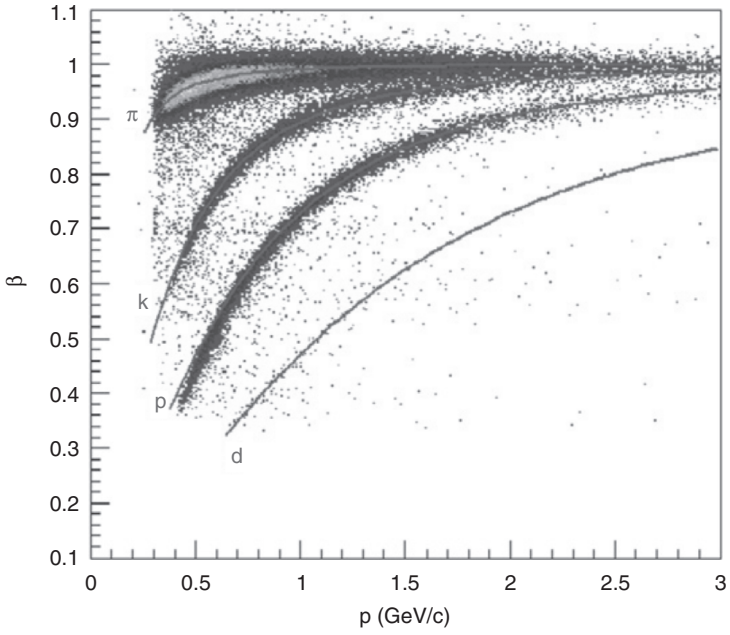

Figure 12.21 Particle identification power of the ALICE MRPC time-of-flight detector (Akindinov *et al*., 2012). By kind permission of Elsevier.

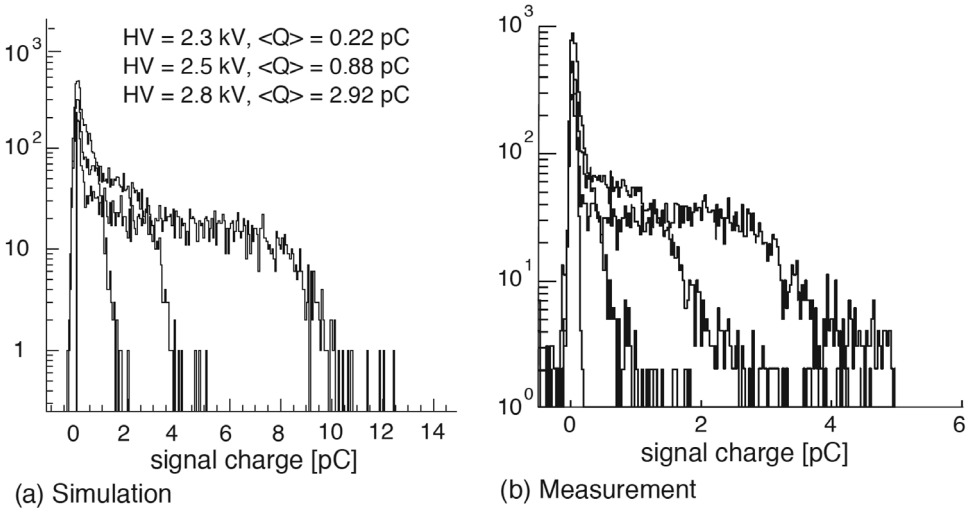

Figure 12.22 Simulated and measured total detected charge for a narrow gap RPC at three values of applied voltage (Lippmann and Riegler, 2004). By kind permission of Elsevier.

https://doi.org/10.1017/9781009291200.014 Published online by Cambridge University Press

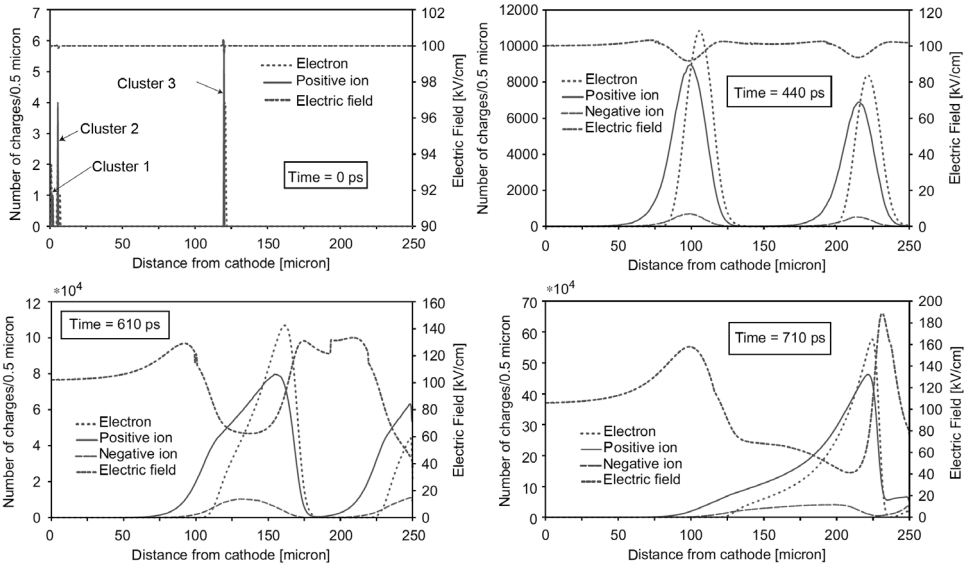

Figure 12.23 Simulation of the charge density evolution with time in an MRPC gap (Doroud *et al.*, 2009a). By kind permission of Elsevier.

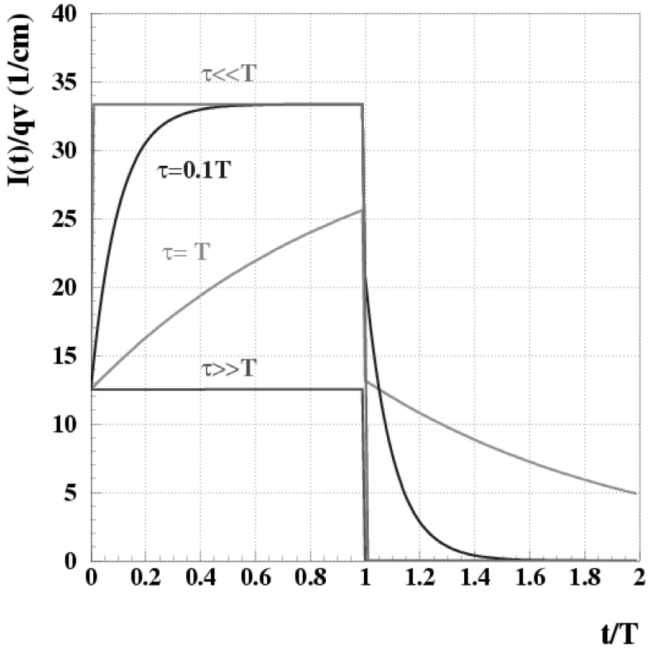

Figure 12.24 Current induced by the avalanche on an external electrode for several values of the time constants (see text) (Riegler, 2002b). By kind permission of Elsevier.

https://doi.org/10.1017/9781009291200.014 Published online by Cambridge University Press

reduce the amount of charge in the gas gap, a possible explanation for the unexpectedly high rate capability of the MRPC.

The time development of the signals induced on external electrodes can be described with the help of the Ramo theorem, already discussed in Chapter 6. For the case of RPCs, the algorithms require some adjustments, which take into account the presence of non-metallic resistive electrodes (Abbrescia *et al.*, 1999a; Riegler, 2002b; Riegler, 2004). For a simple detector geometry, a single gas gap between two electrodes, the shape of the signal current recorded on an external grounded electrode depends on the relative values of the avalanche development time T and of the characteristic detector time constant $\tau = \varepsilon_0 R$, where R is the electrode resistivity, see Figure 12.24. Typical values of the time constants for a standard RPC ($R \sim 10^{12}$ Ω cm) are $T \sim 1$ ns and $\tau \sim 1$ ms ($\tau \gg T$) so the plate conductivity has no effect on the signal, that is simply a constant current until full collection of the charge. Amplitudes and distribution of the induced charge on a set of signal pickup strips can be computed with the same algorithms (Riegler, 2002b).

The presence of a lower resistivity coating layer used to distribute the high voltage affects both the signal shape and distribution; the effect has been studied in detail in the development of a structure aiming at reducing the number of strips needed for the readout of micro-pattern gas detectors, exploiting the charge dispersion on thin-layer resistive anodes (Litt, and Meunier, 1973; Dixit *et al.*, 2004).

Further reading

Riegler, W. (2002) Induced signals in resistive plate chambers. *Nucl. Instr. and Meth.* **A491**, 258.

Abbrescia, M. (2004) The dynamic behaviour of Resistive Plate Chambers. *Nucl. Instr. and Meth.* **A533**, 7.

Sharma, A. (2012) Muon tracking and triggering with gaseous detectors and some applications. *Nucl. Instr. and Meth.* **A666**, 98.

Selected conference proceedings

RPC2005 (2006) VIII International Workshop on Resistive Plate Chambers, S. P. Park, R. Santonico and S. Ratti (eds.) *Nucl. Phys. B (Proc. Suppl.)* **158**.

RPC2008 (2009) IX International Workshop on Resistive Plate Chambers, N. K. Mondal, S. P. Ratti and R. Santonico (eds.) *Nucl. Instr. and Meth.* **A602**.

RPC2011 (2012) X International Workshop on Resistive Plate Chambers, N. Herrmann, R. Santonico and S. Ratti (eds.) *Nucl. Instr. and Meth.* **A661 Suppl. 1**.